An experimental and numerical investigation of coarse aggregate settlement in fresh concrete under vibration

Cai, Yuxin; Liu, Qing feng; Yu, Linwen; Meng, Zhaozheng ; Hu, Zhe; Yuan, Qiang ; Šavija, Branko

Citation (APA)
Cai, Y., Liu, Q. F., Yu, L., Meng, Z., Hu, Z., Yuan, Q., & Šavija, B. (2021). An experimental and numerical investigation of coarse aggregate settlement in fresh concrete under vibration. *Cement and Concrete Composites*, *122*, Article 104153. https://doi.org/10.1016/j.cemconcomp.2021.104153

Important note
To cite this publication, please use the final published version (if applicable).
Please check the document version above.

Contents lists available at ScienceDirect

Cement and Concrete Composites

journal homepage: www.elsevier.com/locate/cemconcomp

An experimental and numerical investigation of coarse aggregate settlement in fresh concrete under vibration

Yuxin Cai [a,b], Qing-feng Liu [a,b,*], Linwen Yu [c], Zhaozheng Meng [a,b], Zhe Hu [a,b], Qiang Yuan [d], Branko Šavija [e]

[a] State Key Laboratory of Ocean Engineering, School of Naval Architecture, Ocean and Civil Engineering, Shanghai Jiao Tong University, Shanghai, 200240, China
[b] Shanghai Key Laboratory for Digital Maintenance of Buildings and Infrastructure, Shanghai, 200240, China
[c] College of Materials Science and Engineering, Chongqing University, Chongqing, 400045, China
[d] School of Civil Engineering, Central South University, Changsha, 410075, China
[e] Microlab, Faculty of Civil Engineering and Geosciences, Delft University of Technology, Delft, 2628CN, the Netherlands

A B S T R A C T

Fresh concrete needs vibration to compact, fill the mould and reach a dense state. During the compaction process, coarse aggregates (CAs) tend to settle, affecting the homogeneity and eventually the long-term durability of hardened concrete. In this study, a 3-D, multi-phase numerical model for fresh concrete is developed for better understanding the CA settlement under vibration. The settlement rate of the CA in vibrated concrete is considered based on the Stokes law, and the calibrated rheological parameter of mixtures is determined by the segmented sieving method. The model prediction shows that the vibration time has the greatest effect on CA settlement, followed by the particle size of CAs, whereas the density of CAs and the plastic viscosity of mixtures contribute a little compared with the aforementioned factors. Through experimental tests, the validity of prediction results is well verified. The proposed model provides a new method to understand and estimate the settlement behaviour of CAs.

1. Introduction

In general, concrete comprises cement as a binder, natural sand and gravel as aggregates, and mixing water together with chemical admixtures. With the hydration reaction of cementitious materials, fresh concrete will gradually develop from a viscoplastic cohesive process to a viscoelastic hardening process [1]. The stability of fresh concrete refers to its ability to maintain the uniform distribution of constituents during transport, casting and compacting [2]. In the process of consolidation, vibration helps to remove entrapped air voids and improve the compactness of concrete, but also causes the relative movement and redistribution of various components of mixtures due to the insufficient cohesion and density difference [3,4]. Notably, high-frequency vibration-induced settlement of coarse aggregates (CAs) greatly increases the heterogeneity of fresh concrete [5–7]. At present, among various types of concretes, only self-compacting concrete with optimum flowability and viscosity does not need to be vibrated during placement [8]. It can be seen that the vibrating process still remains a necessary step in most cases.

The rheological behaviour of vibrated fresh concrete has been reported in some previous studies. Tattersall and Baker [9,10] held the view that fresh concrete no longer behaved as a Bingham model when exposed to vibration, but approximately followed a power-law pseudoplastic model with zero yield value. When the shear rate was rather low, it could be considered as a Newtonian fluid. Hu and de Larrard [11] pointed out that vibration greatly decreased the yield stress, and sometimes even made it practically disappear, which caused the CAs to settle. Nevertheless, the plastic viscosity was reduced a little or seemed unaffected sometimes by external vibration. Esmaeilkhanian et al. [12] indicated that vibration would decrease the "internal friction" of concrete mixtures, which promoted sinking of CAs under the action of gravity. Pichler et al. [13] highlighted again that the apparent flowing behaviour of fresh cement-based materials under vibration could be described using a power-law model with shear-thinning nature.

The settlement of CAs has an adverse impact on the surface appearance, design strength and durability of hardened concrete. This

---

may cause significant problems, such as the decline in mechanical strength, increased shrinkage and cracking, and the reduction of chemical erosion resistance, all of which are detrimental to the performance of reinforced concrete structures [14–21]. However, due to the opacity of concrete, the direct observation of CA settlement with naked eye is impossible. Therefore, some special experimental techniques have been proposed to characterize the settlement phenomenon. Petrou et al. [22] introduced a radioactive element labelling method that utilized nuclear medicine technology to monitor the deposition of CAs in vibrated concrete. Koch et al. [23] and Tian et al. [24] used carbomer gel to prepare a transparent paste, and visually observed the settlement and segregation of fresh concrete. After concrete hardening, Barbosa et al. [25], Navarrete and Lopez [26], and Nili et al. [27] cut the specimen and analysed the CA distribution through image processing. Benaicha et al. [28] proposed a method based on the ultrasonic velocity to estimate the homogeneity and quality of concrete at early age. Through the electrical conductivity method, Khayat et al. [29] inserted the electrode pairs at different heights of concrete specimen to assess the uniformity of CA content. Furthermore, a technique of gamma-ray attenuation was adapted by Vanhove et al. [30] and Gokce et al. [31] to measure the distribution of CAs in concrete.

In summary, the instability caused by vibration is a critical issue in fresh concrete, and it is necessary to present a convenient and visual methodology to reveal the problem of CA settlement in vibrated concrete. In recent years, the theoretical models of rheological properties of cement-based materials have been extensively studied [32–37]. However, these developments have not been applied on the evaluation of CA settlement, and most knowledge is still based on experimental observations described above.

Therefore, the main objective of this study is to develop a rational and reliable numerical model to investigate the settlement of CAs. Experiments are also designed to verify the validity of the model prediction, based on the segmented sieving method. Parametric studies of influencing factors such as the vibration time, the properties of CAs and the plastic viscosity of mixtures on CA settlement are performed and discussed, and grey relational analysis is put forward to compare the influence level of these factors. The proposed model for CA settlement can not only save time, workload and raw materials, but also provide a potential approach to visualize the CA movement and a complementary tool to adequately understand and estimate the settlement behaviour of CAs in vibrated concrete.

2. Experimental details

2.1. Materials and mixtures

P.O 42.5R ordinary Portland cement (OPC) conforming to Chinese standard GB 175–2007 with a density of 3020 kg/m^3 and a Blaine specific surface area of 340 m^2/kg was used to prepare the concrete mixtures. Silica fume (SF), with a density of 2200 kg/m^3 and a Blaine specific surface area of 22205 m^2/kg, was used to replace a certain amount of OPC. The chemical compositions of OPC and SF determined by X-ray fluorescence (XRF) are given in Table 1. River sand was used as the fine aggregate, with the apparent density of 2690 kg/m^3, and the fineness modulus of 2.9. Crushed limestone with a particle size of 5–20 mm was used as the CA, with an apparent density of 2670 kg/m^3 and approximately regular spherical shape. Particle size distribution of raw materials is presented in Fig. 1, where OPC and SF were measured by laser granulometry, and river sand and limestone CA were measured by
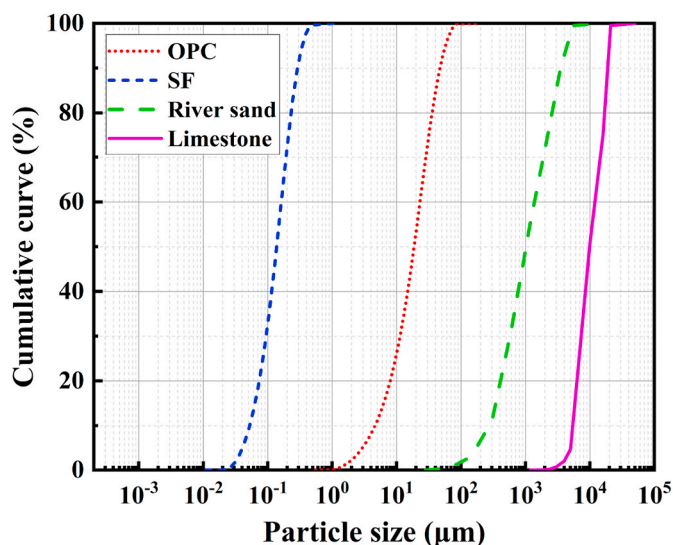
Fig. 1. Particle size distribution of raw materials.

sieving method. High-performance polycarboxylate superplasticizer was used in the mixtures to adjust the workability. Its specific gravity, water reduction rate, solid content and pH were equal to 1.09, 40%, 42% and 6.7, respectively.

Prior works [9–11] showed that vibration could change the rheological behaviour of fresh concrete from a thixotropic fluid with yield stress to a non-thixotropic fluid with a very low or even negligible yield stress value. At this time, the CA settlement mainly depended on the plastic viscosity of mixtures and had no relation to the yield stress [8,22,38,39], and a higher viscosity helped decrease the settlement velocity of CAs [40,41]. Hence, three concrete mixtures with different plastic viscosities were designed by adjusting the dosage of SF. The mix proportions of concrete shown in Table 2 were obtained through multiple experiments. Among them, the first was normal concrete (NC), and the second and third added SF to replace 5% and 10% of OPC by mass, respectively, to obtain mixtures with higher plastic viscosities. The water to binder ratio (w/b) was controlled at 0.40, and the dosage of superplasticizer was 0.5% of cementitious materials by mass.

2.2. Properties of fresh concrete

The main properties of these three groups of concrete mixtures are listed in Table 3. The apparent density, air content, slump, slump flow and bleeding rate were tested according to the Chinese standard GB/T 50080-2016. The rheological parameters of fresh concrete were measured by the ICAR concrete rheometer produced in Denmark. In the flow curve test, the initial speed is 0.50 rps, the final speed is 0.05 rps, the number of testing points is 7, and the duration of each point is 5 s. The yield stress and plastic viscosity of concrete mixtures were calculated from the flow curve based on the Bingham model, as shown in Eq. (1).

$$\tau = \tau_0 + \eta_p \dot{\gamma} \tag{1}$$

where τ is the shear stress, τ_0 is the yield stress, η_p is the plastic viscosity, and $\dot{\gamma}$ is the shear rate.

Table 1
Chemical compositions of OPC and SF (wt%).

Cementitious materials	CaO	SiO$_2$	Al$_2$O$_3$	Fe$_2$O$_3$	MgO	SO$_3$	Alkali content	Loss on ignition
OPC	58.99	22.02	6.19	2.65	2.53	2.67	0.70	3.08
SF	0.76	87.42	0.29	1.75	2.49	0.48	–	3.30

Table 2
Mix proportions of concrete (kg/m^3).

Group	w/b	OPC	SF	River sand	Limestone	Water	Superplasticizer
NC	0.40	400.0	–	736.0	1104.0	160.0	2.0
NC-5%SF	0.40	380.0	20.0	736.0	1104.0	160.0	2.0
NC-10%SF	0.40	360.0	40.0	736.0	1104.0	160.0	2.0

Table 3
Main properties of fresh concrete.

Group	Apparent density (kg/m^3)	Air content (%)	Slump (mm)	Slump flow (mm)	Bleeding rate (%)	Yield stress (Pa)	Plastic viscosity (Pa·s)
NC	2410	2.5	185	530	5.7	466.2	45.0
NC-5%SF	2400	2.3	175	510	4.9	527.9	48.4
NC-10%SF	2395	2.2	160	490	4.3	560.5	51.3

2.3. Evaluation of CA settlement

A method of segmented sieving was put forward to evaluate the settlement of CAs in the experiment. The schematic diagram of experimental steps is exhibited in Fig. 2. Here, a prismatic wooden mould with a cross section of 150 mm × 150 mm and a height of 500 mm was customized. The wooden boards were fixed by bolts, and the joints were coated with silicone gel to prevent leakage. A poker vibrator was used for vibrating and compacting, and its basic parameters are given in Table 4. The specimens were vibrated for 5 s, 15 s and 25 s, respectively. Note that the effective working radius of the vibrator used in experiment is 500 mm, which is much larger than the cross-sectional size of specimen, and the vibrating rod moves across the entire cross section to work during the vibration. Therefore, it is assumed that the vibration energy does not attenuate within the range of specimen, that is, the vibration amplitude and frequency of all particles in fresh concrete are approximately the same.

In the test, the right amount of fresh concrete was poured into the mould. After the vibration, the top of the mould was covered with a wooden board and fastened with bolts. Then the mould was slowly rotated by 90° from the original position, and the side wall was taken off. Next, four pieces of metal slides were inserted vertically along the designed iron grooves. The concrete mixtures were equally divided in five layers along the casting direction. Subsequently, the cover and partitions were removed in proper order. Concrete mixtures of each layer were poured into a 4.75 mm sieve to rinse to remove mortars.

Table 4
Basic parameters of the poker vibrator.

Type	Rod length (mm)	Rod diameter (mm)	Power (W)	Amplitude (mm)	Frequency (Hz)
YFY-01-35	1000	35	900	0.8	230

Finally, the residual CAs were dried and weighed to calculate the CA mass percentage of each layer in the specimen (see Eq. (2)).

$$p_i = \frac{m_i}{M} (i = 1, 2, 3, 4, 5)$$ (2)

where P_i is the mass percentage of CAs in the i-th layer, m_i is the mass of CAs in the i-th layer, and M is the total mass of all CAs in the specimen.

2.4. Analysis of experimental results

Fig. 3 illustrates the results of CA distribution along casting direction measured by the segmented sieving method. In order to eliminate the experimental errors and ensure the repeatability of this method, each test result was determined by the average of multiple groups of fresh concrete mixtures. It could be observed that, during the vibrating procedure, CAs were gradually deposited to the bottom layer of concrete
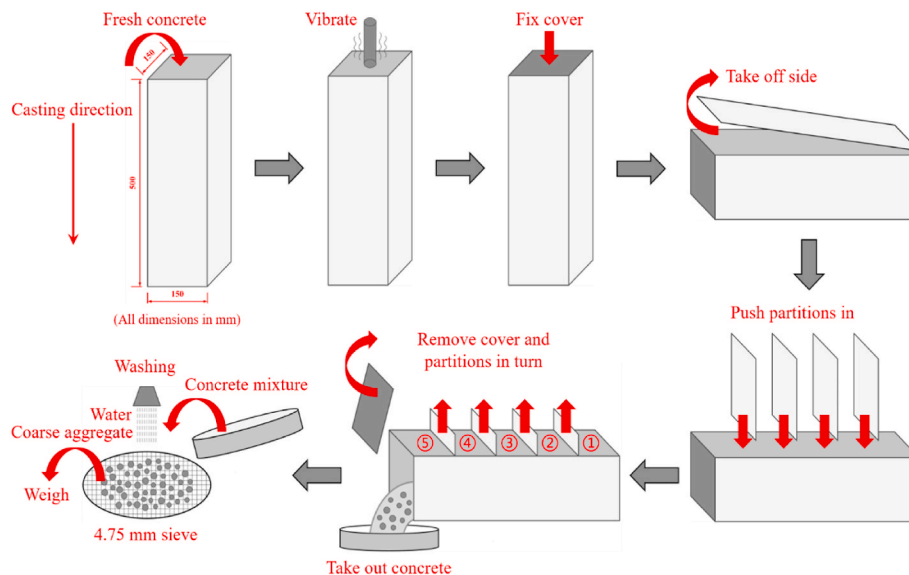
Fig. 2. Testing procedure of segmented sieving method.
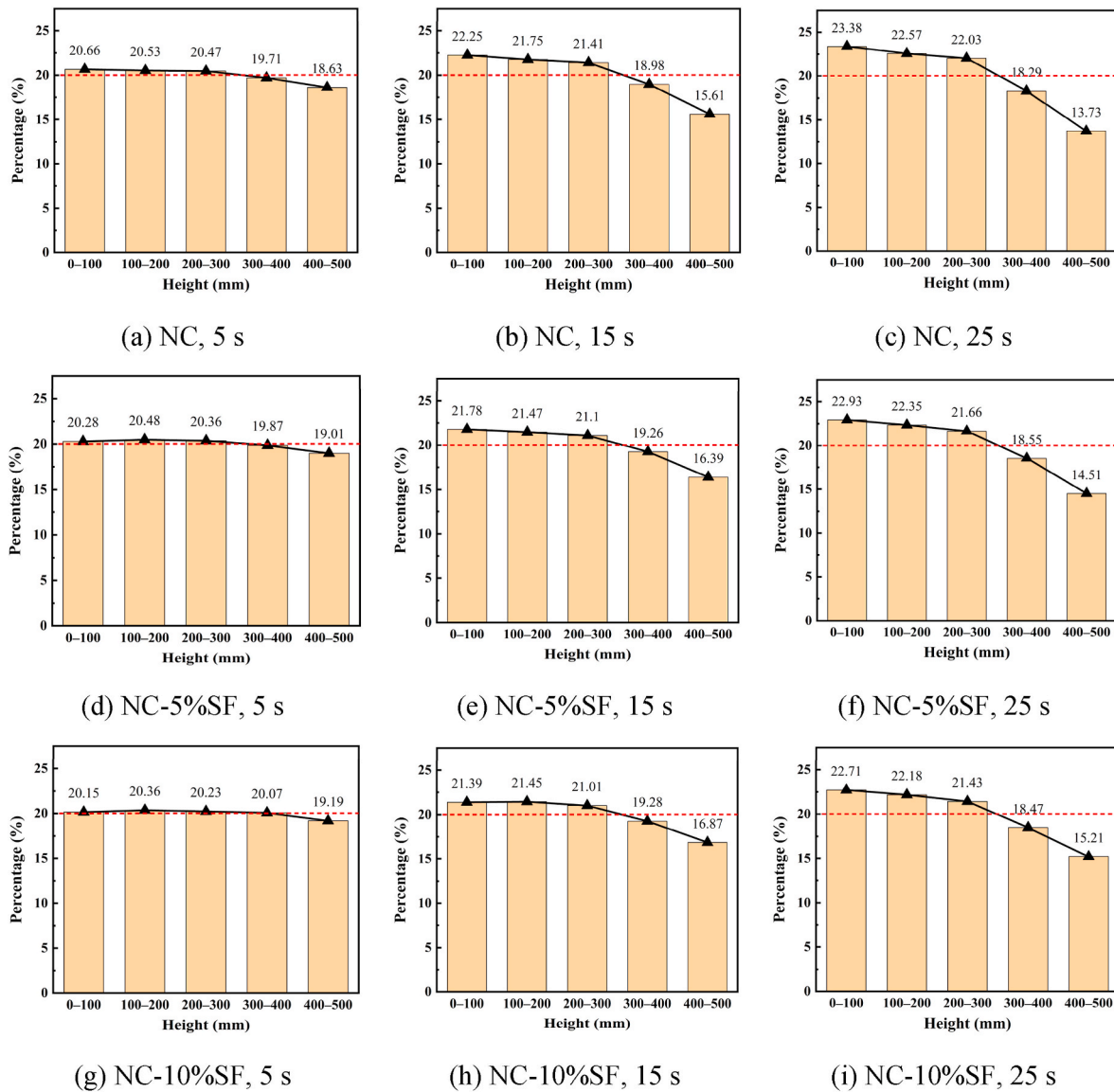
Fig. 3. Experimental results of CA settlement.

mixtures under the action of gravity. At the same time, cement pastes and bleeding water migrated upwards because of the buoyancy. After vibrating, settlement caused a significant decrease in CA content of the top two layers. For the bottom part of specimen, the content of CAs increased, but the variation was not as obvious as the reduction in the top part. It was because a part of CAs gradually formed the close packing in the bottom area after settling for a certain distance. The subsequent CAs accumulated in the middle part of specimen, causing the CA mass percentages of the second and third layers to be close to that of the first layer. The usage of SF could increase the plastic viscosity of fresh cementitious materials [42–44]. It improved the stability of fresh concrete and mitigated the settlement of CAs to a certain extent. Besides, the larger dosage of SF had a more significant mitigation effect on sedimentation phenomenon.

The degree of CA settlement is defined by the standard deviation of the CA mass percentage of each layer in the specimen, calculated according to Eq. (3). It can reflect the overall distribution of CAs, and the higher value indicates that the settlement and heterogeneous distribution of CAs are more significant.

$$S = \sqrt{\frac{\sum_{i=1}^{n} \left(P_i - \overline{P} \right)^2}{n}} \times 1000 \qquad (3)$$

where S is the degree of settlement, P_i is the mass percentage of CAs in the i-th layer, $\overline{P}$ is the average of CA mass percentage of each layer, which is 20%, and n is the number of layers, which is 5.

The variation of the settlement degree of CAs with vibration time is displayed in Fig. 4. It could be clearly understood from the figure that once vibration started, CAs appeared unevenly distributed along the casting direction, and the heterogeneity of CA distribution progressively increased. Adding SF into the concrete mixtures could enhance the plastic viscosity, and reduce the settlement degree by 12.67%–45.33% compared with NC. In addition, a part of CAs formed the dense packing and stopped moving in the bottom part of specimen after a certain period of vibrating, thereby the increase in the degree of CA settlement gradually weakened with the vibration time.
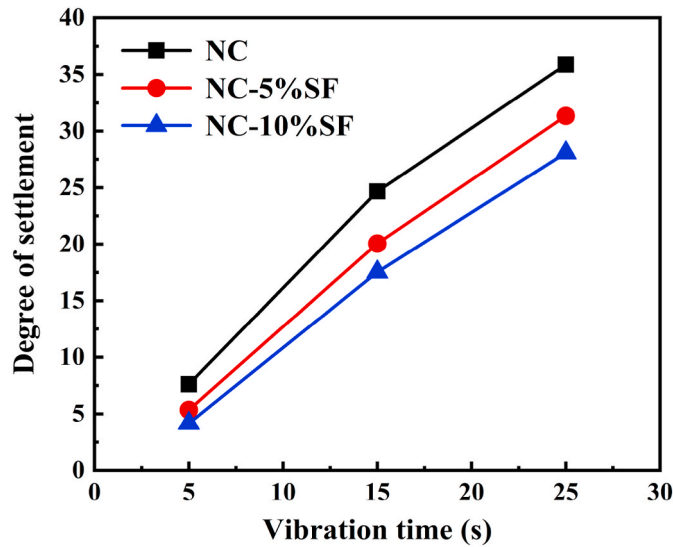
Fig. 4. Experimental results of the degree of CA settlement.

3. Numerical model

3.1. Modelling approach

Numerical studies can provide accurate models at multiple scales to reflect the material compositions and meso/micro structures of concrete [45–48]. In this study, a 3-D fresh concrete model is established at mesoscopic level, as shown in Fig. 5(a). The concrete is considered as a two-phase composite comprising CAs and mortars to facilitate the understanding of the settlement behaviour of CAs. The size of geometric model of the prismatic concrete specimen is 150 mm × 150 mm × 500 mm. The particle size of spherical CAs in the model is 5–20 mm, which is randomly generated according to the Fuller curve, and the volume fraction of CAs is 45%. These parameters are the same as the experiments.

Due to the relatively large size of the model, it contains too much CAs, which will block each other in the line of sight. For easier direct observation of the process of CA settlement, we extract some 2-D slices
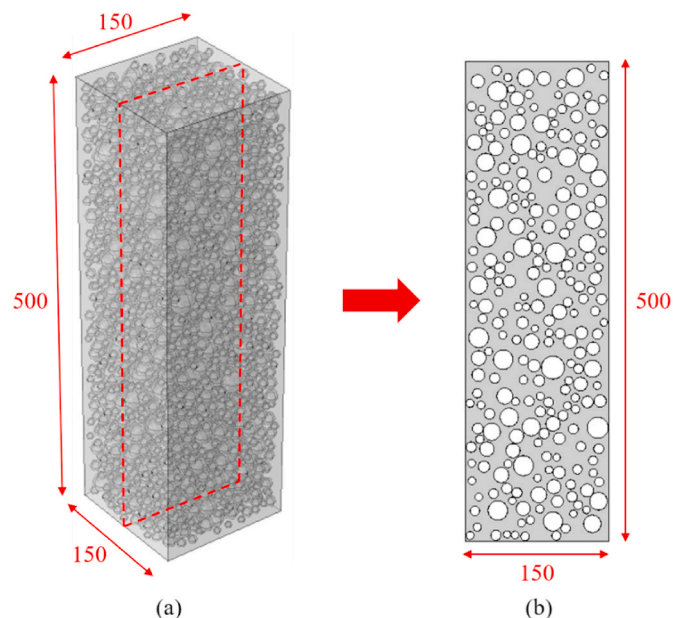
from the 3-D model along the vertical direction and find that the CA settlement in each slice is similar. In consequence, a slice in the middle of 3-D model is extracted vertically for the visual analysis (see Fig. 5(b)). Of course, the calculation of CA content distribution is still based on the 3-D model. It can be seen from the figure that after casting and before vibrating, CAs are randomly and uniformly distributed in concrete.

It is generally believed that the yield stress can prevent CAs from settling in an undistrubed mortar matrix [22,39], but the yield stress is known to decrease to a very low value or even disappear at vibrating state and the plastic viscosity plays a decisive role in the settlement of CAs at this time [9–11,49,50]. Assuming that the yield stress is reduced to zero, a single CA particle is mainly subjected to three forces: gravity, buoyancy and viscous resistance in vibrated mortars. The force analysis of the CA is presented in Fig. 6.

Gravity (*G*) and buoyancy (*B*) can be expressed as:

$$G = \rho_a V g = \frac{1}{6}\pi\rho_a d^3 g \tag{4}$$

$$B = \rho_m V g = \frac{1}{6}\pi\rho_m d^3 g \tag{5}$$

Here, ρ_a and ρ_m are the apparent densities of CAs and mortars, respectively. In the experiment, ρ_a is 2670 kg/m³, and ρ_m is measured on a mortar sample, which is extracted from fresh concrete using a 4.75 mm sieve immediately after the completion of the mixing procedure. The apparent densities of mortars corresponding to the three groups of concrete mixtures are 2285 kg/m³, 2270 kg/m³ and 2260 kg/m³, respectively. *d* is the diameter of CA particle in the range of 5–20 mm, and *g* is the acceleration due to gravity, which is 9.8 N/kg.

Stokes law describes the viscous resistance of a spherical object in the viscous fluid. The following assumptions hold: (1) the liquid extends infinitely, that is, the influence of container wall on the fluid movement is not considered; (2) the object is spherical and moves in a straight line with a constant velocity without deformation during the movement; (3) the velocity of liquid on the surface of the sphere relative to the centre is zero; (4) when the Reynolds number (Re) is small, the inertial effect can be ignored. Here, Re is a dimensionless parameter that distinguishes the flow type of fluid and it can be calculated as:

$$\mathrm{Re} = \frac{\rho_l v d}{\eta} \tag{6}$$

where ρ_l is the fluid density, *v* is the sphere velocity, *d* is the sphere diameter, and η is the fluid viscosity.

When Re is less than 1, the flow is considered to be streamlined; when Re is greater than 10^3, the flow is turbulent; when Re is between the two, the flow is transitional. In concrete mixtures, the movement

Fig. 5. Schematic diagram of geometric model (all dimensions in mm).
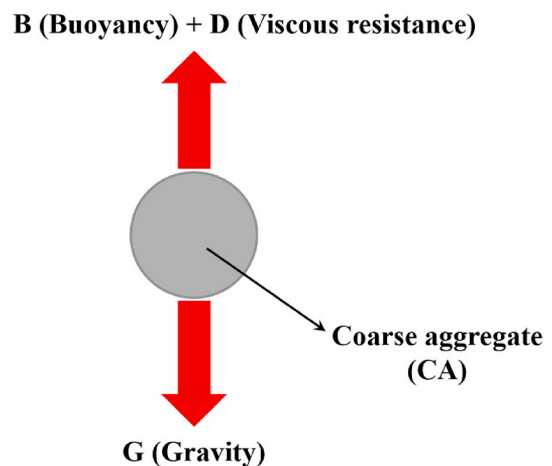
Fig. 6. Force analysis of the CA in vibrated mortars.

velocity of CA particles is extremely slow, and Re is much lower than 1. So the flow around the CA particles is streamlined, and the expression of the viscous resistance (D) is:

$$D = 3\pi\eta v d \tag{7}$$

From the above analysis, it can be seen that when the density of the CA is greater than that of the mortars, the CA will move downwards with acceleration, and the viscous resistance also increases because of the increased CA velocity. When the resultant force of viscous resistance, gravity and buoyancy reaches an equilibrium, the CA will settle at a constant velocity. The final velocity can be demonstrated as:

$$v_s = \frac{d^2 g(\rho_a - \rho_m)}{18\eta_{pl}} \tag{8}$$

where v_s is the final velocity of the CA, and η_{pl} is the plastic viscosity of mortars.

The CA in vibrated mortars can be divided into a varying accelerated motion with a decreasing acceleration and a uniform motion. Through integral calculation, the relationship between the vertical settlement height and the vibration time can be derived as:

$$\begin{aligned} \Delta h &= \frac{d^2 g(\rho_a - \rho_m)}{18\eta_{pl}} \cdot t - \frac{d^4 g \rho_a(\rho_a - \rho_m)}{324\eta_{pl}^2} \cdot \left[1 - \exp\left(-\frac{18\eta_{pl}}{d^2\rho_a} \cdot t\right)\right] \\ &= \frac{d^2 g(\rho_a - \rho_m)}{18\eta_{pl}} \cdot \left\{t - \frac{d^2\rho_a}{18\eta_{pl}} \cdot \left[1 - \exp\left(-\frac{18\eta_{pl}}{d^2\rho_a} \cdot t\right)\right]\right\} \end{aligned} \tag{9}$$

where Δh is the settlement height of the CA, and t is the vibration time.

Since the particle size of CAs in this study is 0.005–0.02 m, the constant and exponential terms in Eq. (9) are much smaller than the linear term. It can be seen that the CA will accelerate to the final velocity in a rather short time, which can be ignored. Moreover, Petrou et al. [39] find that, after the vibration, the yield stress of mortars is restored immediately, and the dynamic CA will stop moving with a great acceleration and stabilize in a static state. Hence, the distance of this deceleration motion can also be ignored. It means that the CA settlement can be approximately regarded as a uniform motion in the whole process of vibration, and its movement distance is expressed as:

$$\Delta h = \frac{d^2 g(\rho_a - \rho_m)}{18\eta_{pl}} \cdot t \tag{10}$$

Eq. (10) shows the settlement height of a single CA in vibrated mortars. But, in fact, each CA particle is also subjected to the interaction from other ones. In this case, the plastic viscosity of mortars can be approximately replaced by that of concrete mixtures, so as to consider the interaction between the CA particles [51–53]. Furthermore, the plastic viscosity of fresh concrete measured in Section 2.2 needs to be calibrated, because the Bingham model is no longer completely suitable to characterize the rheology of fresh cement-based materials under the action of vibration. Consequently, the settlement height of the CA can be revised to:

$$\Delta h' = \frac{d^2 g(\rho_a - \rho_m)}{18k\eta_{pl}'} \cdot t \tag{11}$$

In Eq. (11), $\Delta h'$ is the actual settlement height of the CA, η_{pl}' is the plastic viscosity of fresh concrete, and k is the non-dimensional calibration coefficient for η_{pl}'. The specific value of k will be determined in Section 3.2, which is related to the raw materials and experimental conditions.

3.2. Model calibration

Theoretically, the final height position of a single CA after settlement can be expressed by Eq. (12) through the previous calculation and derivation.

$$h' = h - \frac{d^2 g(\rho_a - \rho_m)}{18k\eta_{pl}'} \cdot t \tag{12}$$

where h is the initial height position of the CA, and h' is the final height position of the CA after settlement.

It should be noted that the CAs with different particle sizes have a different settlement rate [38], which will cause some of them to intersect in the model. To this end, the whole vibration process is divided into many short-time parts, and the vibration time of each step is set as 0.05 s. The final settlement model is generated by superposition of each part step by step, until the expected vibration time is reached. At the end of each part, if the CAs intersect, the involved ones are randomly bounced to the nearby empty space and ensure that they will not intersect with other CAs again. Considering that the CAs will be wrapped with a layer of pastes (interfacial transition zone) with a thickness of 20–50 μm [54–56], the minimum distance between the CA surfaces is set as 100 μm in this study.

In the model, the parameter information of every CA particle can be easily determined at any time and any position. The 3-D model is equally divided into five layers along the height direction, and all CAs are distributed in each layer based on the final position of the centre height of them. According to Eq. (13), the CA volume percentage of each layer in the model can be calculated.

$$P_i' = \frac{V_i}{V} (i = 1, 2, 3, 4, 5) \tag{13}$$

where P_i' is the volume percentage of CAs in the i-th layer, V_i is the volume of CAs in the i-th layer, and V is the total volume of all CAs in the model.

Since the density of all CAs is the same, the volume percentage of CAs in each layer (P_i') can be fitted with the mass percentage (P_i) according to the experimental results of Fig. 3 to calculate the calibration coefficient (k) used in Eq. (11). The algorithm flow chart of k and correlation coefficient (R^2) is presented in Fig. 7. R^2 is calculated by the linear fitting function of software. It can be predicted that the value of R^2 will increase firstly and then decrease with the increase of k, that is, there is a peak value of R^2. When R^2 reaches its maximum value, the algorithm ends. It is found that when k is 0.62, the results of numerical model and experiment are in the best agreement. In that case, R^2 is 0.9865. The original data comparison between the model and experimental results is shown in Table 5, and the fitting result is shown in Fig. 8. The fitting function is self-set as $y=x$, and the abscissa and ordinate represent the results of experiment and numerical model, respectively. Note that k is less than 1. It means that vibration reduces the plastic viscosity of fresh concrete compared to that in the stable state, which is in keeping with earlier findings [11,49,50].

Taking the group of NC as an example, firstly, a 3-D geometric model was generated, and then a 2-D slice was extracted to facilitate the visual observation of CA settlement, as depicted in Fig. 9. As the vibration progressed, CAs gradually deposited to the bottom part of specimen, and the distribution profiles presented an increased content of CAs towards the bottom layer. For a single CA, the CA with a larger particle size showed a more notable settlement distance.

It was noteworthy that the CA content in the top part of specimen was significantly decreased, especially when the vibration time reached 25 s, there were most of mortars and only few of small-sized CAs in the top 50 mm-height area (see Fig. 9(c)). Megid and Khayat [57] observed similar phenomena in their experiment. The settlement of CAs led to the formation of a porous surface layer enriched in cement pastes in the top part of concrete specimen, where might be prone to experience shrinkage and cracking [58,59]. In addition, it could be clearly seen from the figure that CAs in the bottom part indeed formed a close packing in the local space, which confirmed the previous interpretation of the experimental results.

On the basis of the 3-D model, the volume percentages of CAs in the

Fig. 7. Algorithm flow chart.

4. Prediction and discussion

The settlement of CAs is a common phenomenon in fresh concrete due to vibration, and the visually method can provide an important and effective way to reveal the settlement behaviour of CAs. Based on the numerical approach proposed in this study, a corresponding 3-D model can be established to predict the degree of CA settlement under different influencing factors, for example, the vibration time, the apparent density and particle size of CAs, and the plastic viscosity of mixtures. It not only has the advantages of convenience and visualization, but also can further make a theoretical explanation for such a rheological problem in vibrated concrete.

4.1. Influence of vibration time

The distribution of CAs along casting direction under different vibration time is shown in Fig. 11. The orange, green, purple, yellow and blue histograms in the figure represent the volume percentages of CA content from the first layer to the fifth layer of the total, respectively. And the line chart shows the standard deviation of the CA volume percentages of these five layers to characterize the degree of CA settlement (like Eq. (3)). An obvious impact of vibration time on CA settlement could be observed. As the vibrating duration became longer, the
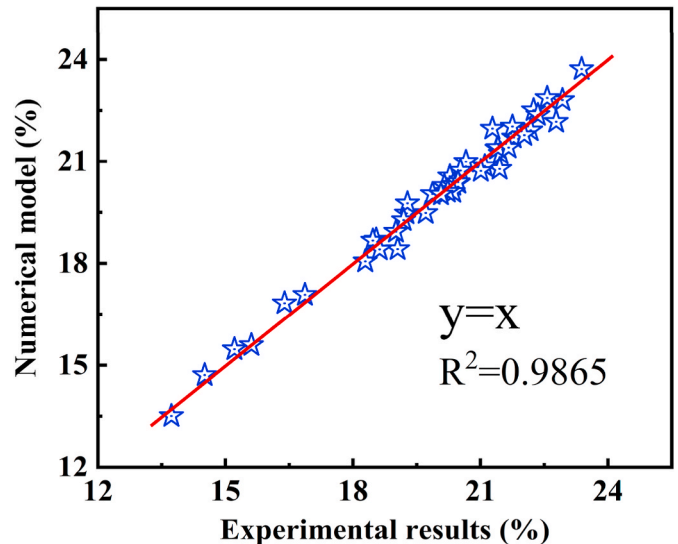
Fig. 8. Fitting between numerical model and experimental results.

five layers were calculated, as illustrated in Fig. 10. Evidently, as the vibration time increased, the heterogeneity of CA distribution along casting direction was gradually strengthened, which was reflected in the obvious decrease of CA content in the top part and the increase of that in the bottom part. This was consistent with the direct observation shown in Fig. 9. Besides, for concrete mixtures having different w/b or mix proportions, as long as the relevant rheological parameter of mixtures and raw material information were input into the model, the CA settlement behaviour could also be easily displayed. The proposed methodology had potential application prospects in large-scale structural concrete cast in practice and 3-D printed concrete.

Table 5
Comparison of the percentage of CA distribution between the model and experiment.

Vibration time	Layer	NC		NC-5%SF		NC-10%SF	
		Model	Experiment	Model	Experiment	Model	Experiment
5 s	1	20.99%	20.66%	20.56%	20.28%	20.28%	20.15%
	2	20.73%	20.53%	20.37%	20.48%	20.31%	20.36%
	3	20.39%	20.47%	20.10%	20.36%	20.11%	20.23%
	4	19.48%	19.71%	20.04%	19.87%	20.03%	20.07%
	5	18.41%	18.63%	18.93%	19.01%	19.27%	19.19%
15 s	1	22.51%	22.25%	21.71%	21.78%	21.38%	21.39%
	2	22.03%	21.75%	21.23%	21.47%	21.05%	21.45%
	3	21.40%	21.41%	20.86%	21.10%	20.72%	21.01%
	4	18.47%	18.98%	19.47%	19.26%	19.77%	19.28%
	5	15.59%	15.61%	16.73%	16.39%	17.08%	16.87%
25 s	1	23.72%	23.38%	22.81%	22.93%	22.27%	22.71%
	2	22.87%	22.57%	22.37%	22.35%	21.92%	22.18%
	3	21.78%	22.03%	21.41%	21.66%	21.67%	21.43%
	4	18.06%	18.29%	18.70%	18.55%	18.67%	18.47%
	5	13.57%	13.73%	14.71%	14.51%	15.47%	15.21%
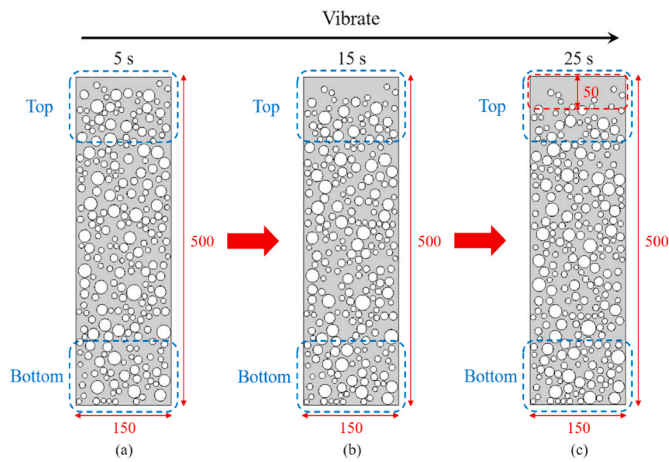
Fig. 9. Visual analysis of CA settlement under vibration (all dimensions in mm).
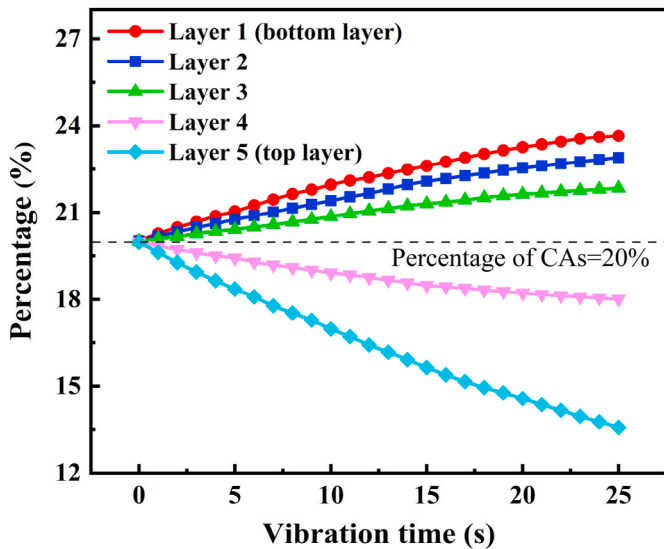
Fig. 10. The CA volume percentages of these five layers in NC.
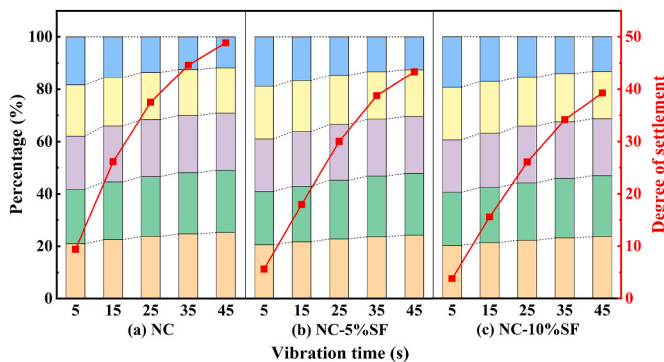
Fig. 11. Influence of the vibration time on CA settlement.

heterogeneity of CA distribution gradually increased. After vibrating for a certain period of time, due to the dense packing of some CAs in the bottom part of specimen, the growing trend of settlement degree became slower. It should be noted that the addition of SF would delay the initial time of that a part of CAs in the bottom area formed a close packing.

In engineering practice, long-time vibration should be avoided,

because excessive vibration would aggravate the settlement, segregation and bleeding of fresh concrete. On the contrary, too short vibration time might make it difficult for each component in mixtures to combine closely and entrapped air voids could not be completely removed from the surface of specimen, which also might affect the quality of hardened concrete. Therefore, when casting fresh concrete, the vibration time should be strictly controlled, usually 20–30 s.

4.2. Influence of CA apparent density

The properties of CAs, such as apparent density, particle size distribution and appearance shape, may all have a certain influence on the degree of settlement [12,38,60–68]. Considering that the laboratory could offer additional CAs with apparent densities of 2520 kg/m³ and 2790 kg/m³, a numerical model of the influence of apparent density on settlement was carried out, and the vibration time was set as 25 s. From Fig. 12, it showed that the CAs with a larger apparent density presented a higher difference between the densities of the CA and the mortar matrix, resulting in a greater sedimentation tendency. This was in line with the finding of Navarrete and Lopez [61], who believed that the settlement rate had a linear relationship with the density difference between CAs and mortars for a given mixture. Furthermore, Chia et al. [62] and Ke et al. [63] studied the settlement behaviour of lightweight CA concrete under vibration. They claimed that when the density of CAs was less than that of the mortars, the CAs would appear to float.

4.3. Influence of CA particle size

In Fig. 13, three particle size distributions of CAs were designed, namely 5–16 mm, 5–20 mm and 9.5–20 mm, and the vibration time was also 25 s. The reason for distinguishing the range of particle size in this way was that it could be easily obtained through the sieves of 9.5 mm and 16 mm sizes in the laboratory, which was beneficial to the subsequent experimental verification. Under the action of vibration, the mixtures which contained more large-sized CAs had a greater degree of settlement for the same CA volume fraction, that was, the distribution of CAs in concrete presented a more evident non-uniformity. This was consistent with the results of Safawi et al. [38]. In their experiment, the CAs with particle sizes of 5–13 mm and 13–20 mm were used to prepare fresh concrete mixtures, respectively. The results showed that the large-sized CAs were more affected due to vibration than the small-sized ones. It meant that the larger-sized CAs were more dominant in determining the settlement degree compared with smaller ones. Similarly, Esmaeilkhanian et al. [12] and Shen et al. [64] also found that concrete mixtures with lower maximum size CAs tended to settle and segregate less.

Moreover, compared with the particle size distribution of CAs which increased from 5–20 mm to 9.5–20 mm, the increase in the settlement degree of the particle size from 5–16 mm to 5–20 mm was more obvious. It was because, although the particle size of CAs increased in both cases,
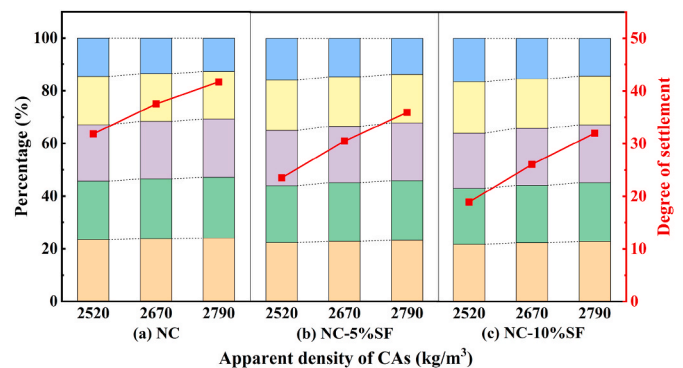
Fig. 12. Influence of the apparent density of CAs on settlement.
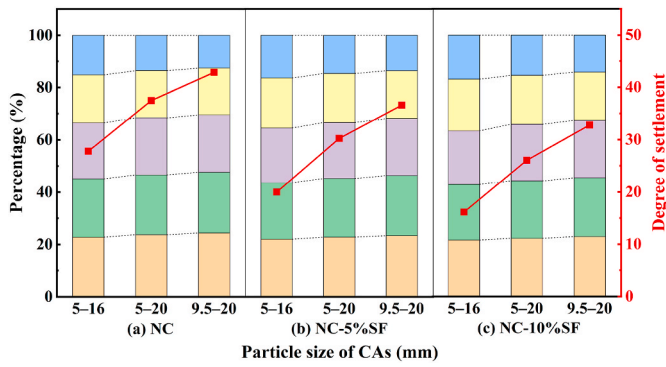
Fig. 13. Influence of the particle size of CAs on settlement.

the CAs with a larger particle size were more likely to form a dense packing when they deposited in the bottom part of specimen, which could prevent the settlement movement to a certain extent.

4.4. Verification of prediction results

In Sections 4.1–4.3, the numerical model was used to predict the influence of vibration time, apparent density and particle size of CAs on settlement degree in the three groups of concrete mixtures. Next, the validity of the proposed model based on experimental results would be discussed in this section. Although the vibration time of fresh concrete usually did not exceed 30 s, the tests of vibrating durations of 35 s and 45 s were still carried out to validate the previous prediction. In addition, the limestone with apparent densities of 2520 kg/m^3 and 2790 kg/m^3 prepared in the laboratory could be used to test the influence of the CA density on settlement. For the experiment of the effect of the CA particle size, the CAs with diameters of 5–16 mm and 9.5–20 mm could

be obtained from original particle size (5–20 mm) through 16 mm and 9.5 mm size sieves, respectively.

The experimental results determined by the segmented sieving method were used to verify the prediction results of numerical model, as presented in Fig. 14. For the vibration time, the model prediction was in good agreement with the experimental results as evident in Fig. 14(a). With the vibration time going on, both the settlement degree and heterogeneity distribution of CAs were more pronounced. When the vibration time reached a certain value, the increase of settlement degree became slower due to the close packing of some CAs in the bottom layer. Similarly, when the numerical method was used to predict the influence of the apparent density and particle size of CAs on settlement, it also showed a good correlation with the experimental results (see Fig. 14(b) and (c)), which indicated that the model was applicable in this study.

4.5. Grey relational analysis

The grey relational analysis table of different influencing factors is summarized in Table 6. Here, this method is used to characterize the contribution of each factor to CA settlement. The settlement degree is taken as the reference sequence. The influencing factors such as vibration time, apparent density and particle size of CAs, and plastic viscosity of mixtures are taken as the comparable sequences.

Assuming the reference and comparable sequences are respectively denoted as $X_0(k)$ and $X_i(k)$. Before conducting a grey relational analysis, the original reference and comparable sequences need to be normalized by data pre-processing, as follows:

$$x_0(k) = \frac{X_0(k)}{\frac{1}{n}\sum_{k=1}^{n} X_0(k)} \tag{14}$$
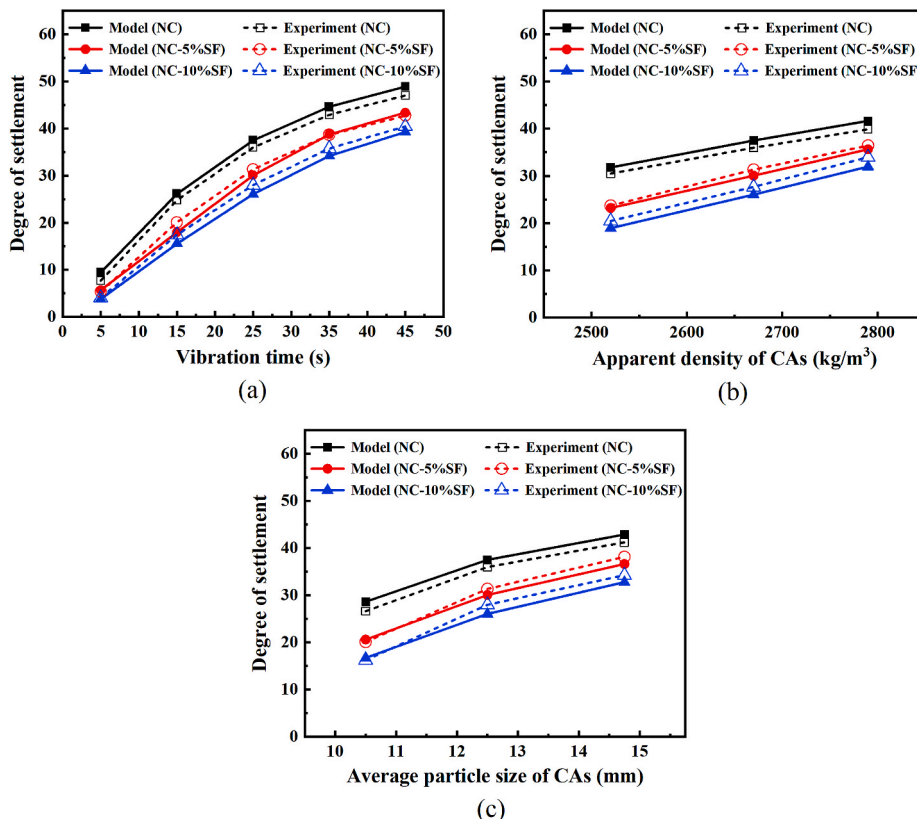
Fig. 14. Experimental verification of the prediction results.

Table 6
Grey relational analysis table of different influencing factors.

Group	Vibration time (s)	Apparent density of CAs (kg/m^3)	Particle size of CAs (mm)	Plastic viscosity of mixtures (Pa·s)	Degree of settlement
1	5	2670	5–20	45.0	9.45
2	15	2670	5–20	45.0	26.14
3	25	2670	5–20	45.0	37.51
4	35	2670	5–20	45.0	44.60
5	45	2670	5–20	45.0	48.88
6	5	2670	5–20	48.4	5.67
7	15	2670	5–20	48.4	17.97
8	25	2670	5–20	48.4	30.06
9	35	2670	5–20	48.4	38.75
10	45	2670	5–20	48.4	43.33
11	5	2670	5–20	51.3	3.80
12	15	2670	5–20	51.3	15.56
13	25	2670	5–20	51.3	26.05
14	35	2670	5–20	51.3	34.15
15	45	2670	5–20	51.3	39.25
16	25	2520	5–20	45.0	31.81
17	25	2790	5–20	45.0	41.65
18	25	2520	5–20	48.4	23.20
19	25	2790	5–20	48.4	35.64
20	25	2520	5–20	51.3	18.94
21	25	2790	5–20	51.3	31.97
22	25	2670	5–16	45.0	28.02
23	25	2670	9.5–20	45.0	42.88
24	25	2670	5–16	48.4	20.30
25	25	2670	9.5–20	48.4	36.62
26	25	2670	5–16	51.3	16.42
27	25	2670	9.5–20	51.3	32.78
Grey relational grade	0.7392	0.6291	0.6435	0.6222	–

$$x_i(k) = \frac{X_i(k)}{\frac{1}{n}\sum_{k=1}^{n} X_i(k)} \tag{15}$$

where $x_0(k)$ and $x_i(k)$ are the sequences after data pre-processing, and $i = 1, 2, …, m$ and $k = 1, 2, …, n$.

When the dimensionless data are prepared, the grey relational coefficient can be derived by Eq. (16).

$$\varepsilon_i(k) = \frac{\Delta_{\min} + \rho\Delta_{\max}}{\Delta_{0i}(k) + \rho\Delta_{\max}} \tag{16}$$

Here, the absolute difference between each evaluated comparable sequence and the corresponding element of reference sequence is calculated in turn, and then $\Delta_{\min}$, $\Delta_{\max}$ and $\Delta_{0i}(k)$ can be obtained by Eqs. (17)–(19). Moreover, ρ is called the resolution coefficient, and the smaller ρ indicates the greater resolution. In general, the value of ρ is 0.5.

$$\Delta_{\min} = \min_{i} \min_{k} |x_0(k) - x_i(k)| \tag{17}$$

$$\Delta_{\max} = \max_{i} \max_{k} |x_0(k) - x_i(k)| \tag{18}$$

$$\Delta_{0i}(k) = |x_0(k) - x_i(k)| \tag{19}$$

As the calculated relational coefficients are not only large in quantity, but also discrete, it is impossible to directly compare them. It needs to average the relational coefficients to convert each sequence into a relational grade, as shown in Eq. (20).

$$\gamma_i = \frac{1}{n}\sum_{k=1}^{n} \varepsilon_i(k) \tag{20}$$

where γ_i is the grey relational grade.

On the basis of the principle of grey relational analysis, a larger value of γ_i implies that the related influencing factor has a greater impact on CA settlement. After calculation, it is found that the grey relational grades of the influencing factors are γ (vibration time) = 0.7392, γ (apparent density of CAs) = 0.6291, γ (particle size of CAs) = 0.6435, and γ (plastic viscosity of mixtures) = 0.6222, respectively. It means that the order of these four influencing factors for the contribution of CA settlement in this study is vibration time > particle size of CAs > apparent density of CAs > plastic viscosity of mixtures. This supports the general observation that vibration time should be limited in practical applications.

5. Conclusions

In this study, an experimental and numerical work of CA settlement in vibrated fresh concrete was investigated. Based on the previous results and discussion, the following conclusions could be drawn:

1) The distribution profiles of CAs in vibrated concrete presented a growing tendency towards the bottom layer with vibration time. After a certain period of vibrating, some CAs in the bottom part formed the close packing, and the growth of the non-uniform distribution gradually began to weaken.
2) Due to the opacity of concrete, the proposed 3-D model for fresh concrete could be used as a potential approach to visualize the CA movement. For the top part of specimen, the visual analysis showed that a surface layer enriched in cement mortars formed in this area, where only contained few of small-sized CAs.
3) The heterogeneity of concrete had a positive correlation with the density difference between CAs and mortars and the particle size of CAs. SF, as a mineral admixture to improve the plastic viscosity of mixtures, could effectively reduce the settlement and segregation of fresh cement-based materials.
4) The segmented sieving method was performed to assess the validity of numerical model. The results indicated that the model prediction was well verified by the experimental results. The methodology proposed in this study provided an effective tool to further understand the settlement behaviour of CAs.
5) Grey relational analysis demonstrated that the vibration time had the greatest influence on CA settlement, followed by the particle size of CAs. Compared with the former two influencing factors, the apparent

density of CAs and the plastic viscosity of mixtures contributed a little to the settlement.

Declaration of competing interest

The authors declare that they have no known competing financial interests or personal relationships that could have appeared to influence the work reported in this paper.

Acknowledgments

References

[1] K. Kovler, N. Roussel, Properties of fresh and hardened concrete, Cement Concr. Res. 41 (7) (2011) 775–792.

[2] N. Roussel, A theoretical frame to study stability of fresh concrete, Mater. Struct. 39 (1) (2006) 81–91.

[3] D. Jiao, C. Shi, Q. Yuan, X. An, Y. Liu, H. Li, Effect of constituents on rheological properties of fresh concrete-A review, Cement Concr. Compos. 83 (2017) 146–159.

[4] G. Torelli, J.M. Lees, Fresh state stability of vertical layers of concrete, Cement Concr. Res. 120 (2019) 227–243.

[5] W.S. Alyhya, S. Kulasegaram, B.L. Karihaloo, Simulation of the flow of self-compacting concrete in the V-funnel by SPH, Cement Concr. Res. 100 (2017) 47–59.

[6] J. Zhang, X. Gao, Y. Su, Influence of poker vibration on aggregate settlement in fresh concrete with variable rheological properties, J. Mater. Civ. Eng. 31 (7) (2019), 04019128.

[7] W. Yan, W. Cui, L. Qi, Effect of aggregate gradation and mortar rheology on static segregation of self-compacting concrete, Construct. Build. Mater. 259 (2020) 119816.

[8] M.I. Safawi, I. Iwaki, T. Miura, A study on the applicability of vibration in fresh high fluidity concrete, Cement Concr. Res. 35 (9) (2005) 1834–1845.

[9] G.H. Tattersall, P.H. Baker, The effect of vibration on the rheological properties of fresh concrete, Mag. Concr. Res. 40 (143) (1988) 79–89.

[10] G.H. Tattersall, P.H. Baker, An investigation into the effect of vibration on the workability of fresh concrete using a vertical pipe apparatus, Mag. Concr. Res. 41 (146) (1989) 3–9.

[11] C. Hu, F. de Larrard, The rheology of fresh high-performance concrete, Cement Concr. Res. 26 (2) (1996) 283–294.

[12] B. Esmaeilkhanian, K.H. Khayat, A. Yahia, D. Feys, Effects of mix design parameters and rheological properties on dynamic stability of self-consolidating concrete, Cement Concr. Compos. 54 (2014) 21–28.

[13] C. Pichler, R. Rock, R. Lackner, Apparent power-law fluid behavior of vibrated fresh concrete: engineering arguments based on Stokes-type sphere viscometer measurements, J. Non-Newtonian Fluid Mech. 240 (2017) 44–55.

[14] W. Zhu, J.C. Gibbs, P.J.M. Bartos, Uniformity of in situ properties of self-compacting concrete in full-scale structural elements, Cement Concr. Compos. 23 (1) (2001) 57–64.

[15] A. Leemann, B. Munch, P. Gasser, L. Holzer, Influence of compaction on the interfacial transition zone and the permeability of concrete, Cement Concr. Res. 36 (8) (2006) 1425–1433.

[16] D.K. Panesar, B. Shindman, The effect of segregation on transport and durability properties of self consolidating concrete, Cement Concr. Res. 42 (2) (2012) 252–264.

[17] X. Gao, J. Zhang, Y. Su, Influence of vibration-induced segregation on mechanical property and chloride ion permeability of concrete with variable rheological performance, Construct. Build. Mater. 194 (2019) 32–41.

[18] Y. Cai, W. Zhang, L. Yu, M. Chen, C. Yang, R. François, K. Yang, Characteristics of the steel-concrete interface and their effect on the corrosion of steel bars in concrete, Construct. Build. Mater. 253 (2020) 119162.

[19] W. Zhang, R. François, Y. Cai, J.-P. Charron, L. Yu, Influence of artificial cracks and interfacial defects on the corrosion behavior of steel in concrete during corrosion initiation under a chloride environment, Construct. Build. Mater. 253 (2020) 119165.

[20] Y. Cai, W. Zhang, C. Yang, R. François, L. Yu, M. Chen, H. Chen, H. Yang, Evaluating the chloride permeability of steel–concrete interface based on concretes of different stability, Struct. Concr. (2020) 1–14.

[21] C. Wu, C. Chen, C. Cheeseman, Size effects on the mechanical properties of 3D printed plaster and PLA parts, J. Mater. Civ. Eng. 33 (7) (2021), 04021152.

[22] M.F. Petrou, K.A. Harries, F. Gadala-Maria, V.G. Kolli, A unique experimental method for monitoring aggregate settlement in concrete, Cement Concr. Res. 30 (5) (2000) 809–816.

[23] J.A. Koch, D.I. Castaneda, R.H. Ewoldt, D.A. Lange, Vibration of fresh concrete understood through the paradigm of granular physics, Cement Concr. Res. 115 (2019) 31–42.

[24] Z. Tian, X. Li, F. Zhu, Z. Peng, Experimental simulation study on aggregate motion of rheological concrete, J. Build. Mater. 19 (1) (2016) 22–28.

[25] F.S. Barbosa, A.L. Beaucour, M.C.R. Farage, S. Ortola, Image processing applied to the analysis of segregation in lightweight aggregate concretes, Construct. Build. Mater. 25 (8) (2011) 3375–3381.

[26] I. Navarrete, M. Lopez, Understanding the relationship between the segregation of concrete and coarse aggregate density and size, Construct. Build. Mater. 149 (2017) 741–748.

[27] M. Nili, M. Razmara, M. Sadeghi, M. Razmara, Automatic image analysis process to appraise segregation resistance of self-consolidating concrete, Mag. Concr. Res. 70 (8) (2018) 390–399.

[28] M. Benaicha, O. Jalbaud, X. Roguiez, A.H. Alaoui, Y. Burtschell, Prediction of Self-Compacting Concrete homogeneity by ultrasonic velocity, Alex. Eng. J. 54 (4) (2015) 1181–1191.

[29] K.H. Khayat, T.V. Pavate, J. Assaad, C. Jolicoeur, Analysis of variations in electrical conductivity to assess stability of cement-based materials, ACI Mater. J. 100 (4) (2003) 302–310.

[30] Y. Vanhove, C. Djelal, G. Schwendenmann, P. Brisset, Study of self consolidating concretes stability during their placement, Construct. Build. Mater. 35 (2012) 101–108.

[31] H.S. Gokce, B.C. Ozturk, N.F. Çam, O. Andiç-Çakir, Gamma-ray attenuation coefficients and transmission thickness of high consistency heavyweight concrete containing mineral admixture, Cement Concr. Compos. 92 (2018) 56–69.

[32] F. Mahmoodzadeh, S.E. Chidiac, Rheological models for predicting plastic viscosity and yield stress of fresh concrete, Cement Concr. Res. 49 (2013) 1–9.

[33] J. Peng, D. Deng, Z. Liu, Q. Yuan, T. Ye, Rheological models for fresh cement asphalt paste, Construct. Build. Mater. 71 (2014) 254–262.

[34] V. Mechtcherine, S. Shyshko, Simulating the behaviour of fresh concrete with the Distinct Element Method – deriving model parameters related to the yield stress, Cement Concr. Compos. 55 (2015) 81–90.

[35] K. Vance, G. Sant, N. Neithalath, The rheology of cementitious suspensions: a closer look at experimental parameters and property determination using common rheological models, Cement Concr. Compos. 59 (2015) 38–48.

[36] B. Il Choi, J.H. Kim, T.Y. Shin, Rheological model selection and a general model for evaluating the viscosity and microstructure of a highly-concentrated cement suspension, Cement Concr. Res. 123 (2019) 105775.

[37] Y. Liu, C. Shi, Q. Yuan, X. An, L. Zhu, B. Wu, The rotation speed-torque transformation equation of the Robertson-Stiff model in wide gap coaxial cylinders rheometer and its applications for fresh concrete, Cement Concr. Compos. 107 (2020) 103511.

[38] M.I. Safawi, I. Iwaki, T. Miura, The segregation tendency in the vibration of high fluidity concrete, Cement Concr. Res. 34 (2) (2004) 219–226.

[39] M.F. Petrou, B.L. Wan, F. Gadala-Maria, V.G. Kolli, K.A. Harries, Influence of mortar rheology on aggregate settlement, ACI Mater. J. 97 (4) (2000) 479–485.

[40] Y.A. Abebe, L. Lohaus, Rheological characterization of the structural breakdown process to analyze the stability of flowable mortars under vibration, Construct. Build. Mater. 131 (2017) 517–525.

[41] T.R. Muzenda, P. Hou, S. Kawashima, T. Sui, X. Cheng, The role of limestone and calcined clay on the rheological properties of LC3, Cement Concr. Compos. 107 (2020) 103516.

[42] D. Kong, D.J. Corr, P. Hou, Y. Yang, S.P. Shah, Influence of colloidal silica sol on fresh properties of cement paste as compared to nano-silica powder with agglomerates in micron-scale, Cement Concr. Compos. 63 (2015) 30–41.

[43] J.J. Assaad, Correlating thixotropy of self-consolidating concrete to stability, formwork pressure, and multilayer casting, J. Mater. Civ. Eng. 28 (10) (2016), 04016107.

[44] S. Zhuang, Q. Wang, Inhibition mechanisms of steel slag on the early-age hydration of cement, Cement Concr. Res. 140 (2021) 106283.

[45] L.-X. Mao, Z. Hu, J. Xia, et al., Multi-phase modelling of electrochemical rehabilitation for ASR and chloride affected concrete composites, Compos. Struct. 207 (2019) 176–189.

[46] Q.-F. Liu, M.F. Iqbal, J. Yang, et al., Prediction of chloride diffusivity in concrete using artificial neural network: modelling and performance evaluation, Construct. Build. Mater. 268 (2021) 121082.

[47] C.-L. Zhang, W.-K. Chen, S. Mu, et al., Numerical investigation of external sulfate attack and its effect on chloride binding and diffusion in concrete, Construct. Build. Mater. 285 (2021) 122806.

[48] W.K. Chen, Q.F. Liu, Moisture and multi-ions transport in concrete under drying-wetting cycles: a numerical study, J. Hydraul. Eng. 52(5) (2021) 622–632.

[49] F. de Larrard, C. Hu, T. Sedran, J.C. Szitkar, M. Joly, F. Claux, F. Derkx, A new rheometer for soft-to-fluid fresh concrete, ACI Mater. J. 94 (3) (1997) 234–243.

[50] P.F.G. Banfill, Y. Xu, P.L.J. Domone, Relationship between the rheology of unvibrated fresh concrete and its flow under vibration in a vertical pipe apparatus, Mag. Concr. Res. 51 (3) (1999) 181–190.

[51] Z. Li, G. Cao, Rheological behaviors and model of fresh concrete in vibrated state, Cement Concr. Res. 120 (2019) 217–226.

[52] J.-Y. Petit, E. Wirquin, Y. Vanhove, K.H. Khayat, Yield stress and viscosity equations for mortars and self-consolidating concrete, Cement Concr. Res. 37 (5) (2007) 655–670.

[53] A. Leemann, F. Winnefeld, The effect of viscosity modifying agents on mortar and concrete, Cement Concr. Compos. 29 (5) (2007) 341–349.

[54] S. Diamond, J.D. Huang, The ITZ in concrete – a different view based on image analysis and SEM observations, Cement Concr. Compos. 23 (2–3) (2001) 179–188.

[55] Q.-F. Liu, D. Easterbrook, J. Yang, L.-Y. Li, A three-phase, multi-component ionic transport model for simulation of chloride penetration in concrete, Eng. Struct. 86 (2015) 122–133.

[56] Q.F. Liu, Multi-phase modelling of concrete at meso-micro scale based on multi-species transport, J. Chin. Ceram. Soc. 46(08) (2018) 1074–1080.

[57] W.A. Megid, K.H. Khayat, Effect of concrete rheological properties on quality of formed surfaces cast with self-consolidating concrete and superworkable concrete, Cement Concr. Compos. 93 (2018) 75–84.

[58] J.J. Assaad, J. Harb, Surface settlement of cementitious-based materials determined by oedometer testing, Mater. Struct. 44 (2011) 845–856.

[59] B.M. Aïssoun, J.-L. Gallias, K.H. Khayat, Influence of formwork material on transport properties of self-consolidating concrete near formed surfaces, Construct. Build. Mater. 146 (2017) 329–337.

[60] Q.-F. Liu, G.-L. Feng, J. Xia, J. Yang, L.-Y. Li, Ionic transport features in concrete composites containing various shaped aggregates: a numerical study, Compos. Struct. 183 (2018) 371–380.

[61] I. Navarrete, M. Lopez, Estimating the segregation of concrete based on mixture design and vibratory energy, Construct. Build. Mater. 122 (2016) 384–390.

[62] K.S. Chia, C.C. Kho, M.H. Zhang, Stability of fresh lightweight aggregate concrete under vibration, ACI Mater. J. 102 (5) (2005) 347–354.

[63] Y. Ke, A.L. Beaucour, S. Ortola, H. Dumontet, R. Cabrillac, Influence of volume fraction and characteristics of lightweight aggregates on the mechanical properties of concrete, Construct. Build. Mater. 23 (2009) 2821–2828.

[64] L. Shen, H.B. Jovein, Q. Wang, Correlating aggregate properties and concrete rheology to dynamic segregation of self-consolidating concrete, J. Mater. Civ. Eng. 28 (1) (2016), 04015067.

[65] M.F. Iqbal, Q.-F. Liu, I. Azim, et al., Prediction of mechanical properties of green concrete incorporating waste foundry sand based on gene expression programming, J. Hazard Mater. 384 (2020) 121322.

[66] J.J. Assaad, Influence of recycled aggregates on dynamic/static stability of self-consolidating concrete, J. Sustainable Cem.-Based Mater. 6 (6) (2017) 345–365.

[67] W. Cui, W.-S. Yan, H.-F. Song, X.-L. Wu, DEM simulation of SCC flow in L-Box set-up: influence of coarse aggregate shape on SCC flowability, Cement Concr. Compos. 109 (2020) 103558.

[68] M.F. Iqbal, M.F. Javed, M. Rauf, et al., Sustainable utilization of foundry waste: forecasting mechanical properties of foundry sand based concrete using multi-expression programming, Sci. Total Environ. 780 (2021) 146524.